



Synthesis and structural characterization of the ternary Zintl phases $AE_3Al_2Pn_4$ and $AE_3Ga_2Pn_4$ ($AE=Ca, Sr, Ba, Eu; Pn=P, As$)

Hua He, Chauntae Tyson, Maia Saito, Svilen Bobev*

Department of Chemistry and Biochemistry, University of Delaware, Newark, DE 19716, USA

ARTICLE INFO

Article history:

Received 14 November 2011

Received in revised form

19 January 2012

Accepted 23 January 2012

Available online 30 January 2012

Keywords:

Crystal structure

Single-crystal X-ray diffraction

Electronic structure calculations

Zintl phases.

ABSTRACT

Ten new ternary phosphides and arsenides with empirical formulae $AE_3Al_2Pn_4$ and $AE_3Ga_2Pn_4$ ($AE=Ca, Sr, Ba, Eu; Pn=P, As$) have been synthesized using molten Ga, Al, and Pb fluxes. They have been structurally characterized by single-crystal and powder X-ray diffraction to form with two different structures— $Ca_3Al_2P_4$, $Sr_3Al_2As_4$, $Eu_3Al_2P_4$, $Eu_3Al_2As_4$, $Ca_3Ga_2P_4$, $Sr_3Ga_2P_4$, $Sr_3Ga_2As_4$, and $Eu_3Ga_2As_4$ crystallize with the $Ca_3Al_2As_4$ structure type (space group $C2/c$, $Z=4$); $Ba_3Al_2P_4$ and $Ba_3Al_2As_4$ adopt the $Na_3Fe_2S_4$ structure type (space group $Pnma$, $Z=4$). The polyanions in both structures are made up of $TrPn_4$ tetrahedra, which share common corners and edges to form ${}^2_\infty[TrPn_2]^{3-}$ layers in the phases with the $Ca_3Al_2As_4$ structure, and ${}^1_\infty[TrPn_2]^{3-}$ chains in $Ba_3Al_2P_4$ and $Ba_3Al_2As_4$ with the $Na_3Fe_2S_4$ structure type. The valence electron count for all of these compounds follows the Zintl–Klemm rules. Electronic band structure calculations confirm them to be semiconductors.

© 2012 Elsevier Inc. All rights reserved.

1. Introduction

In recent years, there have been numerous reports on the crystal chemistry and physical properties of ternary pnictides in the systems $AE-Tr-Pn$ ($AE=Ca, Sr, Ba, Eu, Yb; Tr=Al, Ga, In$; and $Pn=P, As, Sb$). Examples include $BaGa_2Sb_2$ [1], $Yb_5Al_2Sb_6$ [2], $Ba_2In_5As_5$ [3], Eu_3InP_3 [4], $Eu_3In_2P_4$ [5], $EuIn_2P_2$ [6], $EuGa_2As_2$ [7], Ca_3AlSb_3 [8] and $Ca_5Al_2Sb_6$ [9], to name just a few. Almost exclusively, such compounds can be classified as Zintl phases [10], where the alkaline-earth metals are the “cations” and they donate their valence electrons to the post-transition elements, which, in turn, form covalent bonds within (poly)anionic substructure. The electron transfer is typically considered to be “complete”, and all constituent atoms achieve closed-shell configurations [10,11]. These are desirable characteristics in thermoelectrics development, and many research groups are turning their attention to Zintl phases as candidate materials for solid-state energy conversion. Recent papers have already demonstrated the favorable balance of charge and heat-transport properties for the compounds $Yb_5Al_2Sb_6$ [2], and Ca_3AlSb_3 [8]; $EuIn_2As_2$ [12] can be cited as an example showing colossal magnetoresistance.

Our research group has previously explored considerable sections of the ternary $AE-Ga-Sb$ and $AE-In-Sb$ phase diagrams ($AE=Ca, Sr, Ba, Eu$ and Yb). Since these early studies had proven

fruitful [13–16], not long ago, we embarked on investigations of the corresponding arsenide and phosphide systems. For the synthesis of new compounds with novel structures, by and large, we have focused on the metal flux method [17,18], since the triel elements Ga and In are particularly well-suited for such endeavors. Published structures from our prior systematic work include $BaGa_2Pn_2$ ($Pn=P, As$) [19], and $CaGa_2P_2$, $CaGa_2As_2$, and $SrGa_2As_2$ [20], which all crystallize with different structures. Attempts to extend the “1–2–2” chemistry to the $AE-Al-Pn$ system led to the identification of two series of new compounds $AE_3Ga_2Pn_4$ and $AE_3Al_2Pn_4$, which are the subject of this paper. Herein, we present the ten newly synthesized compounds— $Ba_3Al_2P_4$ and $Ba_3Al_2As_4$ with the $Na_3Fe_2S_4$ structure type [21], and $Ca_3Al_2P_4$, $Sr_3Al_2As_4$, $Eu_3Al_2P_4$, $Eu_3Al_2As_4$, $Ca_3Ga_2P_4$, $Sr_3Ga_2P_4$, $Sr_3Ga_2As_4$, and $Eu_3Ga_2As_4$, isostructural with the previously reported $Ca_3Al_2As_4$ [22] and $Sr_3Al_2P_4$ [23]. Their bonding characteristics are elaborated and the topological relationships to the structures of compounds with formulae AE_3TrPn_3 are discussed as well. The electronic band structures, calculated with the aid of the TB-LMTO method [24], are also discussed.

2. Experimental

2.1. Synthesis

All synthetic and post-synthetic manipulations were performed inside an argon-filled glove box or under vacuum. The elements with stated purity greater than 99.9 wt% were purchased from either Alfa Aesar or Aldrich and used as received.

* Corresponding author. Fax: +1 302 831 6335.
E-mail address: bobev@udel.edu (S. Bobev).

All initial reactions were done in a manner, consistent with the synthesis of CaGa_2P_2 , CaGa_2As_2 , and SrGa_2As_2 [20], where excess Ga was utilized as a reactive flux; details of the metal flux method can be found elsewhere [17,18]. Such reactions were aimed at the “missing” members of any of the three structures above, but by serendipity afforded crystals of the new compounds $\text{Ca}_3\text{Ga}_2\text{P}_4$ and $\text{Sr}_3\text{Ga}_2\text{P}_4$. Subsequent to the structure elucidation by single-crystal X-ray diffraction, the syntheses of these three compounds were replicated using mixtures of the corresponding elements with the proper stoichiometric $AE:Pn$ ratio of 3:4 and a 25-fold excess of Ga. The mixtures of the elements were loaded in alumina crucibles, which were then flame-sealed in fused silica tubes under vacuum. The evacuated silica tubes were heated at 960 °C for 20 h, and then cooled to 500 °C at a rate of 5 °C/h. The molten Ga was decanted at this temperature. Previous successful application of Pb flux for the crystal growth of other $AE\text{--Ga--Pn}$ ternary compounds [20] prompted us to undertake Pb flux reactions again. They were done in a similar way, starting with the corresponding elements in the 3:2:4 ratio and a large amount of Pb (20-fold excess)—large single-crystals of $\text{Ca}_3\text{Ga}_2\text{P}_4$, $\text{Sr}_3\text{Ga}_2\text{P}_4$, $\text{Sr}_3\text{Ga}_2\text{As}_4$, and $\text{Eu}_3\text{Ga}_2\text{As}_4$ were obtained from such experiments.

Attempts to synthesize isotypic $\text{Ba}_3\text{Ga}_2\text{P}_4$ and $\text{Ba}_3\text{Ga}_2\text{As}_4$ compounds were unsuccessful—the outcome, depending on the $AE:Pn$ ratio (1:2 or 3:4), and the choice of flux (Ga or Pb) were

BaGa_2P_2 and BaGa_2As_2 [19], or $\text{Ba}_7\text{Ga}_4\text{P}_9$ and $\text{Ba}_7\text{Ga}_4\text{As}_9$ [25], which are isotypic to $\text{Ba}_7\text{Ga}_4\text{Sb}_9$ [26]. $\text{Ca}_3\text{Ga}_2\text{As}_4$ and $\text{Eu}_3\text{Ga}_2\text{P}_4$ are also still unknown and could not be obtained under the studied experimental conditions. In these cases, crystals of CaGa_2As_2 [19], $\text{Ca}_{14}\text{GaAs}_{11}$ [27], and EuGa_4 [28] were obtained. Analogous reactions with Yb afforded only the binary phases YbP, YbAs, GaAs, and GaP [28].

Switching to aluminum as a reactive flux proved to be somewhat more challenging, although we identified six new compounds— $\text{Ba}_3\text{Al}_2\text{P}_4$, $\text{Ba}_3\text{Al}_2\text{As}_4$, $\text{Ca}_3\text{Al}_2\text{P}_4$, $\text{Sr}_3\text{Al}_2\text{As}_4$, $\text{Eu}_3\text{Al}_2\text{P}_4$, and $\text{Eu}_3\text{Al}_2\text{As}_4$. First, the higher melting point of Al metal (660 °C) [29] required the corresponding reactions to be equilibrated at 960 °C for 20 h, and then cooled to 750 °C. Second, since Al is a strong reducing agent and Al vapors are known to react quickly with SiO_2 , extreme care had to be exercised when the ampoules were removed from the furnace and the molten Al was decanted. Third, yields of the title compounds were lower, and AlP or AlAs [28] were common side products; the crystals were also smaller compared to the crystals obtained from analogous Ga flux reactions.

The crystals exhibit characteristic colors, indicative of them being intrinsic semiconductors: $\text{Ca}_3\text{Al}_2\text{P}_4$ is orange; $\text{Sr}_3\text{Al}_2\text{As}_4$, $\text{Ca}_3\text{Ga}_2\text{P}_4$, $\text{Sr}_3\text{Ga}_2\text{P}_4$, and $\text{Ba}_3\text{Al}_2\text{P}_4$ are red; $\text{Eu}_3\text{Al}_2\text{P}_4$ is dark brown; and $\text{Eu}_3\text{Al}_2\text{As}_4$, $\text{Eu}_3\text{Ga}_2\text{As}_4$, $\text{Sr}_3\text{Ga}_2\text{As}_4$, and $\text{Ba}_3\text{Al}_2\text{As}_4$ are black.

2.2. Powder X-ray diffraction

X-ray powder diffraction patterns were collected at room temperature on a Rigaku MiniFlex powder diffractometer using filtered $\text{CuK}\alpha$ radiation ($\lambda = 1.5418 \text{ \AA}$). The diffractometer was enclosed and operated inside a glove-box. The observed peak-positions and the peaks' relative intensities, analyzed using the JADE 6.5 software package, matched well with those calculated from the single-crystal work. According to powder patterns collected for specimens kept under inert atmosphere and to those collected after being exposed to air, all of the title compounds are unstable at ambient conditions. The air-sensitivity was found to vary considerably, with the Ba-containing samples being the most reactive and the Eu-containing samples being the least sensitive, respectively.

2.3. Single-crystal X-ray diffraction

Single-crystal X-ray diffraction data were collected on a Bruker SMART CCD-based diffractometer, employing monochromated $\text{MoK}\alpha$ radiation ($\lambda = 0.71073 \text{ \AA}$). Crystals from freshly prepared samples

Table 1

Selected single-crystal data collection and structure refinement parameters for $\text{Ba}_3\text{Al}_2\text{Pn}_4$ ($Pn = \text{P, As}$).

Empirical formula	$\text{Ba}_3\text{Al}_2\text{As}_4$	$\text{Ba}_3\text{Al}_2\text{P}_4$
Formula weight	765.66	589.86
Temperature	200(2) K	
Radiation, λ	MoK α , 0.71073 Å	
Space group, Z	Pnma (No. 62), 4	
a (Å)	7.425(2)	7.2540(5)
b (Å)	11.784(3)	11.5416(8)
c (Å)	11.842(3)	11.5770(8)
V (Å ³)	1036.0(5)	969.26(12)
ρ_{cal} (g/cm ³)	4.909	4.042
μ (cm ⁻¹)	240.49	128.13
Goodness-of-fit on F^2	1.079	1.106
R_1 ($I > 2\sigma_I$) ^a	0.0348	0.0189
wR_2 ($I > 2\sigma_I$) ^a	0.0664	0.0394
Largest diff. peak/hole ($e^-/\text{Å}^{-3}$)	2.133/−1.453	1.143/−0.777

^a $R_1 = \sum ||F_o| - |F_c|| / \sum |F_o|$; $wR_2 = [\sum [w(F_o^2 - F_c^2)^2] / \sum [w(F_o^2)^2]]^{1/2}$, where $w = 1 / [\sigma^2 F_o^2 + (AP)^2]$, and $P = (F_o^2 + 2F_c^2) / 3$; A—weight coefficient.

Table 2

Selected single-crystal data collection and structure refinement parameters for $\text{AE}_3\text{Al}_2\text{Pn}_4$ ($AE = \text{Ca, Sr, Eu}$; $Pn = \text{P, As}$).

Empirical formula	$\text{Ca}_3\text{Al}_2\text{P}_4$	$\text{Sr}_3\text{Al}_2\text{As}_4$	$\text{Eu}_3\text{Al}_2\text{P}_4$	$\text{Eu}_3\text{Al}_2\text{As}_4$	$\text{Ca}_3\text{Ga}_2\text{P}_4$	$\text{Sr}_3\text{Ga}_2\text{P}_4$	$\text{Sr}_3\text{Ga}_2\text{As}_4$	$\text{Eu}_3\text{Ga}_2\text{As}_4$
Formula weight	298.08	616.5	633.72	809.52	383.56	526.18	701.98	895.00
Temperature	200(2) K							
Radiation, λ	MoK α , 0.71073 Å							
Space group, Z	C2/c (No. 15), 4							
a (Å)	12.6236(11)	13.5017(16)	13.0304(17)	13.404(2)	12.623(3)	13.1522(13)	13.497(3)	13.386(4)
b (Å)	9.8358(8)	10.4565(13)	10.0974(13)	10.3935(17)	9.870(2)	10.1989(10)	10.497(2)	10.426(3)
c (Å)	6.4469(6)	6.8109(8)	6.5857(8)	6.7502(11)	6.4435(15)	6.6290(7)	6.7903(16)	6.732(2)
β (°)	90.454(1)	90.457(2)	90.607(2)	90.023(2)	91.050(3)	90.314(1)	90.275(4)	90.742(4)
V (Å ³)	800.44(12)	961.5(2)	866.45(19)	940.4(3)	802.6(3)	889.19(16)	962.0(4)	939.5(5)
ρ_{cal} (g/cm ³)	2.474	4.259	4.858	5.718	3.174	3.931	4.847	6.327
μ (cm ⁻¹)	29.82	303.42	222.97	338.31	93.24	244.90	356.25	392.88
Goodness-of-fit on F^2	1.053	0.993	1.195	1.038	1.037	1.000	1.001	1.159
R_1 ($I > 2\sigma_I$) ^a	0.0219	0.0325	0.0161	0.0164	0.0187	0.0248	0.0222	0.0185
wR_2 ($I > 2\sigma_I$) ^a	0.0464	0.0528	0.0362	0.0352	0.0419	0.0507	0.0492	0.0430
Largest diff. peak and hole ($e^-/\text{Å}^{-3}$)	0.429/−0.361	1.102/−1.139	0.773/−1.075	0.878/−0.795	0.437/−0.467	0.832/−0.875	0.934/−0.900	0.969/−1.004

^a $R_1 = \sum ||F_o| - |F_c|| / \sum |F_o|$; $wR_2 = [\sum [w(F_o^2 - F_c^2)^2] / \sum [w(F_o^2)^2]]^{1/2}$, where $w = 1 / [\sigma^2 F_o^2 + (AP)^2 + (BP)^2]$, and $P = (F_o^2 + 2F_c^2) / 3$; A, B—weight coefficients.

were selected under a microscope in the glove-box and cut to suitable sizes (ca. 0.1 mm in all dimensions). The crystals were then mounted on glass fibers using Paratone-N oil. The operating temperature was 200(2) K, maintained by a cold nitrogen stream. This method for handling the crystals alleviated the issue with their air-sensitivity. After ensuring the crystal quality, full spheres of data were collected in four batch runs with frame width of 0.4° for ω and θ . Data collection and data integration were done using SMART and SAINT-plus programs, respectively [30]. SADABS was used for semi-empirical absorption correction based on equivalent reflections [31]. The structures were solved by direct methods and refined by full matrix least squares on F^2 using SHELXL [32]. In the last refinement cycles, the unit cell axes and the atomic coordinates were standardized with the aid of the *Structure TIDY* program [33]. All crystal data and refinement parameters are summarized in Tables 1 and 2; positional and equivalent isotropic displacement parameters for representative structures are listed in Tables 3 and 4. Selected interatomic distances and angles are tabulated in Tables 5 and 6. CIFs have also been deposited with Fachinformationszentrum Karlsruhe, 76344 Eggenstein-Leopoldshafen, Germany (fax: +49 7247-808-666; e-mail: hcrysdta@fiz.karlsruhe.de) with depository numbers: CSD-423778 for $\text{Ba}_3\text{Al}_2\text{P}_4$, CSD-423779 for $\text{Ba}_3\text{Al}_2\text{As}_4$, CSD-423780 for $\text{Ca}_3\text{Al}_2\text{P}_4$, CSD-423781 for $\text{Ca}_3\text{Ga}_2\text{P}_4$, CSD-423782 for $\text{Sr}_3\text{Ga}_2\text{P}_4$, CSD-423783 for $\text{Eu}_3\text{Al}_2\text{P}_4$, CSD-423784 for $\text{Eu}_3\text{Ga}_2\text{As}_4$, CSD-423785 for $\text{Sr}_3\text{Ga}_2\text{As}_4$, CSD-423786 for $\text{Eu}_3\text{Al}_2\text{As}_4$, and CSD-423787 for $\text{Sr}_3\text{Al}_2\text{As}_4$.

2.4. Electronic structure calculations

The Stuttgart TB-LMTO 4.7 program [34] was used to calculate band structures of $\text{Ba}_3\text{Al}_2\text{P}_4$, $\text{Ba}_3\text{Al}_2\text{As}_4$, and $\text{Sr}_3\text{Al}_2\text{As}_4$. Local density approximation (LDA) was used to treat exchange and correlations [35]. All relativistic effects except for spin-orbital

Table 3

Atomic coordinates and equivalent isotropic displacement parameters U_{eq}^a (\AA^2) of $\text{Ba}_3\text{Al}_2\text{Pn}_4$ ($\text{Pn}=\text{P}, \text{As}$).

Atom	Wyckoff Site	x	y	z	U_{eq}
$\text{Ba}_3\text{Al}_2\text{P}_4$					
Ba1	8d	0.0788(1)	0.0775(1)	0.1387(1)	0.012(1)
Ba2	4c	0.0961(1)	1/4	0.7656(1)	0.011(1)
Al	8d	0.0591(1)	0.1249(1)	0.4638(1)	0.010(1)
P1	8d	0.1537(1)	0.5571(1)	0.3871(1)	0.011(1)
P2	4c	0.3084(2)	1/4	0.5282(1)	0.011(1)
P3	4c	0.4101(2)	1/4	0.1693(1)	0.010(1)
$\text{Ba}_3\text{Al}_2\text{As}_4$					
Ba1	8d	0.0812(1)	0.0760(1)	0.1377(1)	0.013(1)
Ba2	4c	0.0929(1)	1/4	0.7612(1)	0.012(1)
Al	8d	0.0598(3)	0.1257(2)	0.4623(2)	0.011(1)
As1	8d	0.1587(1)	0.5594(1)	0.3866(1)	0.012(1)
As2	4c	0.3154(2)	1/4	0.5284(1)	0.011(1)
As3	4c	0.4084(2)	1/4	0.1745(1)	0.011(1)

^a U_{eq} is defined as one third of the trace of the orthogonalized U_{ij} tensor.

Table 4

Atomic coordinates and equivalent isotropic displacement parameters U_{eq}^a (\AA^2) of $\text{Sr}_3\text{Al}_2\text{As}_4$. The refined coordinates for the isostructural $\text{AE}_3\text{Al}_2\text{Pn}_4$ ($\text{AE}=\text{Ca}, \text{Eu}; \text{Pn}=\text{P}, \text{As}$) and $\text{Sr}_3\text{Ga}_2\text{As}_4$ are provided as supporting information.

Atom	Wyckoff Site	x	y	z	U_{eq}
$\text{Sr}_3\text{Al}_2\text{As}_4$					
Sr1	8f	0.1219(1)	0.1295(1)	0.5383(1)	0.011(1)
Sr2	4e	0	0.4015(1)	1/4	0.009(1)
Al	8f	0.2952(1)	0.1227(2)	0.0811(3)	0.009(1)
As1	8d	0.1163(1)	0.1755(1)	0.0246(1)	0.009(1)
As2	8f	0.3412(1)	0.0822(1)	0.4258(1)	0.009(1)

^a U_{eq} is defined as one third of the trace of the orthogonalized U_{ij} tensor.

Table 5

Selected interatomic distances (\AA) and angles ($^\circ$) of $\text{Ba}_3\text{Al}_2\text{Pn}_4$ ($\text{Pn}=\text{P}, \text{As}$).

$\text{Ba}_3\text{Al}_2\text{P}_4$			$\text{Ba}_3\text{Al}_2\text{As}_4$		
Ba1–	P3	3.1412(10)	Ba1–	As3	3.2085(12)
	P3	3.2254(11)		As3	3.2857(12)
	P1	3.3127(10)		As1	3.4007(12)
	P2	3.3979(11)		As2	3.4593(12)
	P1	3.4656(10)		As1	3.5316(12)
	P1	3.5080(10)		As1	3.5510(12)
Ba2–	P2	3.1513(13)	Ba2–	As2	3.2138(15)
	P2	3.1708(13)		As2	3.2340(14)
	P1 × (2)	3.1991(9)		As1 × (2)	3.2636(11)
	P1 × (2)	3.3718(9)		As1 × (2)	3.4047(11)
Al–	P3	2.3718(15)	Al–	As3	2.456(3)
	P1	2.3802(14)		As1	2.470(2)
	P2	2.4314(15)		As2	2.521(3)
	P1	2.4444(14)		As1	2.539(2)
	Al	2.888(2)		Al	2.929(5)
	Al	3.122(2)		Al	3.220(4)
P3–Al–P1		115.24(5)	As3–Al–As1		115.05(9)
P3–Al–P2		100.16(5)	As3–Al–As2		101.71(9)
P1–Al–P2		115.08(5)	As1–Al–As2		113.71(9)
P3–Al–P1		111.45(6)	As3–Al–As1		110.84(10)
P1–Al–P1		99.36(5)	As1–Al–As1		100.01(9)
P2–Al–P1		116.33(5)	As2–Al–As1		116.15(9)

Table 6

Selected interatomic distances (\AA) and angles ($^\circ$) of $\text{Sr}_3\text{Al}_2\text{As}_4$.

Sr1–	As2	3.0649(9)	Al–	As2	2.461(2)
	As2	3.1035(10)		As2	2.471(2)
	As1	3.1912(10)		As1	2.505(2)
	As1	3.2764(9)		As1	2.533(2)
	As1	3.3487(10)		Al	3.127(2)
	As1	3.5317(10)	As2–Al–As2		101.36(7)
	Al	3.535(2)	As2–Al–As1		114.84(8)
Sr2–	As2 × (2)	3.0700(7)	As2–Al–As1		111.78(7)
	As2 × (2)	3.1054(9)	As2–Al–As1		107.34(7)
	As1 × (2)	3.2315(9)	As2–Al–As1		118.70(8)
	Al × (2)	3.5907(19)	As1–Al–As1		103.27(7)

coupling were taken into account by the scalar relativistic approximation [36]. The basis set included the 5d, 6s, and 6p orbitals for Ba; 4d, 5s, and 5p orbitals for Sr, 3s, 3p, and 3d orbitals for Al; 4s, 4p, and 4d orbitals for As, and 3s, 3p, and 3d orbitals for P. The 6p orbital of Ba, 5p orbital of Sr, 3d orbital of Al, 4d orbital of As, and 3d orbital of P were treated with the down-folding technique [37]. The k -space integrations were performed by the tetrahedron method [38], using 225–294 irreducible k -points in the Brillouin zone. The total and partial density of states (DOS) were computed and studied. To interrogate the chemical bonding, crystal orbital Hamilton populations (COHP) [39] of selected interactions were also analyzed.

3. Results and discussion

3.1. Structure of $\text{Ba}_3\text{Al}_2\text{P}_4$ and $\text{Ba}_3\text{Al}_2\text{As}_4$

$\text{Ba}_3\text{Al}_2\text{P}_4$ and $\text{Ba}_3\text{Al}_2\text{As}_4$ are isotypic, and crystallize with the orthorhombic space group $Pnma$ (No. 62, Pearson symbol $oP36$) [28]. This structure formally belongs to the $\text{Na}_3\text{Fe}_2\text{S}_4$ structure type, which has been discussed in an earlier publication [21]. The asymmetric unit of the structure contains two Ba, one Al, and three pnictogen atoms, located at either the general site 8d or the special position 4c (Table 3). Al and Pn atoms constitute AlPn_4 tetrahedra, which by sharing common edges form ${}^1_{\infty}[\text{AlPn}_4/2]^{3-}$ chains, as shown in Fig. 1. These chains of edge-shared tetrahedral

units run along the b axis with Ba^{2+} cations separating them. The chains are similar to those commonly found in the structures of the silicon dichalcogenides [40]; they are also seen in Zintl compounds, such as Ba_2ZnPn_2 [41] and Na_3AlAs_2 [42]. However, the ${}^1_{\infty}[\text{AlPn}_2]^{3-}$ chains in $\text{Ba}_3\text{Al}_2\text{P}_4$ and $\text{Ba}_3\text{Al}_2\text{As}_4$ are not isosteric with the ${}^1_{\infty}[\text{SiS}_2]$ chains in SiS_2 [40] or the ${}^1_{\infty}[\text{ZnPn}_2]^{4-}$ chains in Ba_2ZnPn_2 [41], although they are isoelectronic. Instead, the ${}^1_{\infty}[\text{AlPn}_2]^{3-}$ chains “swivel” in space, as if the centers of the AlPn_4 tetrahedra form a zigzag chain [43], while the Si and Zn atoms in the former are arranged in straight lines.

The Al–P and Al–As distances are in the range of 2.372(2)–2.444(2) and 2.456(3)–2.539(2) Å, respectively, which match closely with the sum of the corresponding Pauling’s single-bond radii of Al (1.248 Å) and P (1.10 Å) and As (1.210 Å) [44]. These values also compare well with those reported for other phosphides and arsenides with similar bonding patterns: $d_{\text{Al–P}} = 2.376$ Å in Na_3AlP_2 [45], $d_{\text{Al–As}} = 2.507$ Å in Na_3AlAs_2 [42], $d_{\text{Al–P}} = 2.377$ –2.443 Å in $\text{Sr}_3\text{Al}_2\text{P}_4$ [23], $d_{\text{Al–As}} = 2.503$ –2.540 Å in Ca_3AlAs_3 [46], suggesting strong covalent bonding character.

Ba1 and Ba2 atoms are both surrounded by six pnictogens in distorted octahedral fashion, although the more regular octahedra for Ba2 should be noted. This is not unusual since Ba2 is a higher

symmetry site (4c) than the Ba1 site (8d). On average, the Ba2–Pn distances are slightly shorter than the Ba1–Pn distances—3.244(1) Å vs. 3.342(1) Å in $\text{Ba}_3\text{Al}_2\text{P}_4$ and 3.297(1) Å vs. 3.406(1) Å in $\text{Ba}_3\text{Al}_2\text{As}_4$. In the second coordination sphere of the Ba atoms, the nearest Al neighbors are located more than 3.7 Å away, which is longer than the sum of their Pauling’s atomic radii ($r_{\text{Ba}} = 2.215$ Å and $r_{\text{Al}} = 1.429$ Å [44]), implying negligible Ba–Al interactions.

3.2. Structure of $\text{AE}_3\text{Al}_2\text{P}_4$ and $\text{AE}_3\text{Ga}_2\text{P}_4$ ($\text{AE} = \text{Ca}, \text{Sr}, \text{Eu}; \text{Pn} = \text{P}, \text{As}$)

The rest of the title compounds, $\text{Ca}_3\text{Al}_2\text{P}_4$, $\text{Sr}_3\text{Al}_2\text{As}_4$, $\text{Eu}_3\text{Al}_2\text{P}_4$, $\text{Eu}_3\text{Al}_2\text{As}_4$, $\text{Ca}_3\text{Ga}_2\text{P}_4$, $\text{Sr}_3\text{Ga}_2\text{P}_4$, $\text{Sr}_3\text{Ga}_2\text{As}_4$, and $\text{Eu}_3\text{Ga}_2\text{As}_4$ all crystallize with the monoclinic space group $C2/c$ (No. 15, Pearson symbol $mS36$) [28]. They are isostructural with the previously reported $\text{Ca}_3\text{Al}_2\text{As}_4$ [22] and $\text{Sr}_3\text{Al}_2\text{P}_4$ [23]. For the sake of simplicity in the context of direct comparison with $\text{Ba}_3\text{Al}_2\text{As}_4$, one of these compounds, $\text{Sr}_3\text{Al}_2\text{As}_4$, will be discussed as a representative.

The structure of $\text{Sr}_3\text{Al}_2\text{As}_4$ is based on AlAs_4 tetrahedra, which by both corner- and edge-sharing form ${}^2_{\infty}[\text{AlAs}_2]^{3-}$ layers (Fig. 2), not ${}^1_{\infty}[\text{AlPn}_2]^{3-}$ chains, as in $\text{Ba}_3\text{Al}_2\text{As}_4$. The layers feature 4-membered and 12-membered rings, which are similar to the layers found in the EuGa_2S_4 structure [47]. The Al–As distances are again indicative of

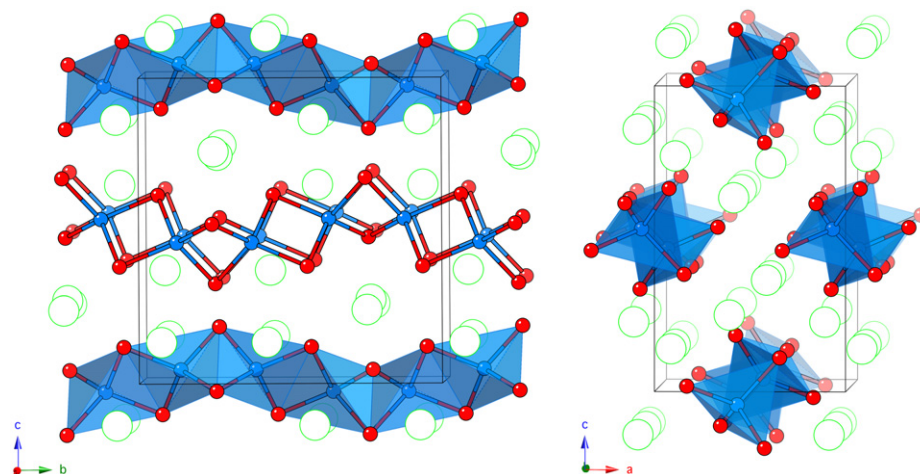


Fig. 1. Combined ball-and-stick and polyhedral representations of the crystal structure of $\text{Ba}_3\text{Al}_2\text{As}_4$, projected along both the a axis and the b axis. The unit cell is outlined. On-line colors: Al atoms are represented as cyan spheres, the pnictogens are drawn as red spheres, and the Ba atoms are shown as green spheres, respectively. (For interpretation of the references to color in this figure, the reader is referred to the web version of this article.)

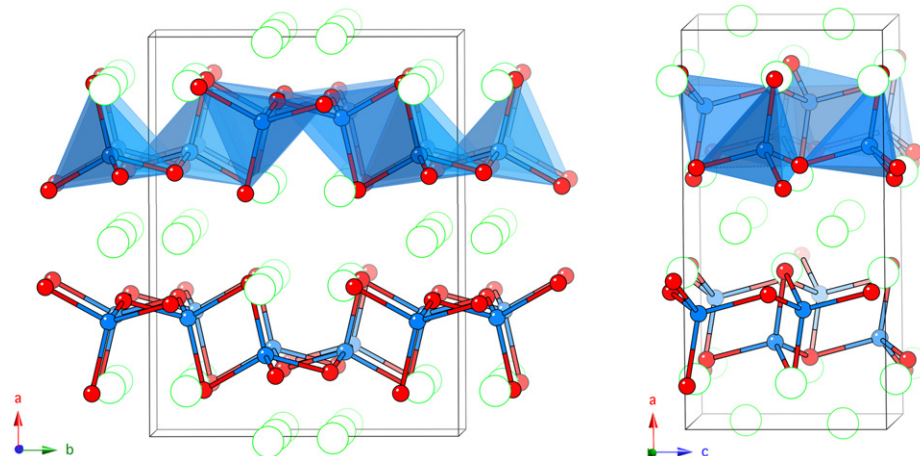


Fig. 2. Combined ball-and-stick and polyhedral representations of the crystal structure of $\text{Sr}_3\text{Al}_2\text{As}_4$, projected along both the b axis and the c axis. On-line colors: Al atoms are represented as cyan spheres, the pnictogens are drawn as red spheres, and the Sr atoms are shown as green spheres, respectively. The unit cell is outlined. (For interpretation of the references to color in this figure, the reader is referred to the web version of this article.)

the covalent character of the Al–As bonding. They are comparable with those in $\text{Ba}_3\text{Al}_2\text{As}_4$. The Al–As distances in the series $\text{Sr}_3\text{Al}_2\text{As}_4$ – $\text{Eu}_3\text{Al}_2\text{As}_4$ – $\text{Ca}_3\text{Al}_2\text{As}_4$ fall in the narrow range 2.415(5)–2.533(2) Å, showing a slight contraction in the presented order. Such decrease can be correlated with the decrease in the corresponding atomic sizes ($r_{\text{Sr}}=2.148$ Å; $r_{\text{Eu}}=2.084$ Å and $r_{\text{Ca}}=1.970$ Å [44]).

Two different Sr sites exist in the structure—Sr1 (between the layers) and Sr2 (within the layers). Sr2 is located in an irregular octahedron of As atoms with an average Sr–As distance of 3.136 Å. On the other hand, Sr1 is only 5-coordinated to As if only the first coordination sphere is considered. However, if another As and the closest Al atom are considered, which are about the same distance away from Sr1, 3.532(1) Å and 3.535(2) Å, respectively, the coordination environment of Sr1 can be described as a monocapped octahedron. This subtle difference in the cationic coordination, which seems to be related to the sizes of the cations (and perhaps to their electronegativities too [44]), could be a reason for $\text{Sr}_3\text{Al}_2\text{As}_4$ and $\text{Ba}_3\text{Al}_2\text{As}_4$ to crystallize with different structure types. Notice that only $\text{Ba}_3\text{Al}_2\text{P}_4$ and $\text{Ba}_3\text{Al}_2\text{As}_4$ crystallize with the $\text{Na}_3\text{Fe}_2\text{S}_4$ structure, and all of the lighter alkaline-earth metal analogs, including $\text{Eu}_3\text{Al}_2\text{P}_4$, $\text{Eu}_3\text{Al}_2\text{As}_4$, $\text{Eu}_3\text{Ga}_2\text{P}_4$, and $\text{Eu}_3\text{Ga}_2\text{As}_4$, adopt the $\text{Ca}_3\text{Al}_2\text{As}_4$ structure.

3.3. Structural relationships

Although the $\text{Ba}_3\text{Al}_2\text{As}_4$ and $\text{Sr}_3\text{Al}_2\text{As}_4$ structures are distinctly different, they share common building motifs – the AlAs_4 tetrahedra – which through different edge- and corner-sharing form two different polyanionic sub-structures. A search of the ICSD database reveals a third structure type adopted by some $\text{AE}_3\text{Tr}_2\text{Pn}_4$ compounds, exemplified by the $\text{Sr}_3\text{In}_2\text{P}_4$ structure (*Pnmm*, No. 58, Pearson symbol *oP18*) [48]. This structure contains another type of edge-shared tetrahedral motifs, which are dimerized and further interconnected by corner sharing (see supporting information). It is interesting to note that breaking down the anionic parts of these three structures results in *TrPn*₃ motifs, which are building blocks in the structures of some AE_3TrPn_3 compounds [46,49,50]. For example, the $^{1}_{\infty}[\text{AlAs}_2]^{3-}$ chain in $\text{Ba}_3\text{Al}_2\text{As}_4$ could be cleaved into dimers of edge-shared AlAs_4 tetrahedra—the very same isolated $[\text{Al}_2\text{Sb}_6]^{12-}$ units are found to exist in the structure of Ba_3AlSb_3 [46]. Both $\text{Sr}_3\text{Al}_2\text{As}_4$ and $\text{Sr}_3\text{In}_2\text{P}_4$ structures can also be cut into edge-shared Al_2As_6 and In_2P_6 fragments if the corner-sharing is removed. On the other hand, the $^{2}_{\infty}[\text{AlAs}_2]^{3-}$ layer and the $^{1}_{\infty}[\text{InP}_2]^{3-}$ chain can also be “broken” along the shared-edges, which will result in infinite 1-D chains of corner-shared tetrahedra—these again have prototypes among some other AE_3TrPn_3 structures (Fig. 3). For example, the $^{1}_{\infty}[\text{InP}_3]^{6-}$ chain derived from $\text{Sr}_3\text{In}_2\text{P}_4$ is a simple one repeating unit chain, which is similar to those found in the Ca_3InP_3 structure [49]. The $^{1}_{\infty}[\text{AlAs}_3]^{6-}$ fragment excised from $\text{Sr}_3\text{Al}_2\text{As}_4$ is a two-unit repeating chain that is similar to $^{1}_{\infty}[\text{GaSb}_3]^{6-}$ seen from Sr_3GaSb_3 [50]. The same arrangement could be seen in the KPO_3 structure [51] too.

3.4. Electron count and electronic structure

Despite the different connectivity of the *TrPn*₄ tetrahedra, these structures are free of *Tr–Tr* or *Pn–Pn* bonds, and the *Tr–Pn* distances suggest that the corresponding interactions are simple 2-center-2-electron bonds. Therefore, following the valence rules and keeping in mind that all of the pnictogen atoms are 2-bonded, the formulae of the title compounds can be readily rationalized as $(\text{AE}^{2+})_3(4b\text{–Tr}^{1-})_2(2b\text{–Pn}^{1-})_4$, i.e., they are Zintl phases [11]. Electronic structure calculations (below) confirm this reasoning.

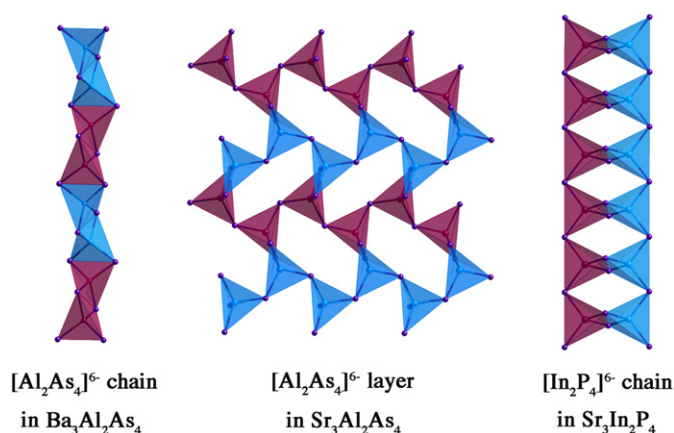


Fig. 3. Comparative representation of fragments from the polyanionic sub-structures of $\text{Ba}_2\text{Al}_2\text{As}_4$ ($\text{Na}_3\text{Fe}_2\text{S}_4$ structure type), $\text{Sr}_3\text{Al}_2\text{As}_4$ ($\text{Ca}_3\text{Al}_2\text{As}_4$ structure type), and $\text{Sr}_3\text{In}_2\text{P}_4$ (own structure type).

Tight-binding linear-muffin-tin-orbital (TB-LMTO-ASA) electronic structure calculations were carried out for $\text{Ba}_3\text{Al}_2\text{P}_4$, $\text{Ba}_3\text{Al}_2\text{As}_4$, and $\text{Sr}_3\text{Al}_2\text{As}_4$. The plots of the computed density of states (DOS) and the crystal orbital Hamilton populations (COHP) for each compound are shown in Figs. 4 and 5, respectively. Band gaps can be noticed at the Fermi level in each DOS plot, suggesting that these compounds are intrinsic semiconductors, as expected for Zintl phases. The sizes of the band gaps in $\text{Ba}_3\text{Al}_2\text{P}_4$ and $\text{Ba}_3\text{Al}_2\text{As}_4$ are calculated to be on the order of 1.6 and 1.3 eV, respectively, which is in good agreement with the difference in electronegativities of P and As [44]. The band gap of $\text{Sr}_3\text{Al}_2\text{As}_4$ is also ca. 1.6 eV. Considering that the LMTO calculations usually underestimate the band gap in semiconductor, these values actually correlate reasonably well with the colors of the crystals ($\text{Sr}_3\text{Al}_2\text{As}_4$ and $\text{Ba}_3\text{Al}_2\text{P}_4$ being red; $\text{Ba}_3\text{Al}_2\text{As}_4$ being dark-to-black).

In spite of the different structure types, contributions from the elements to the states around the Fermi level are similar. In the energy window from -3.5 eV to the Fermi edge (0 eV), the states originate predominantly from the *p* orbitals of pnictogens and Al; a substantial contribution from the *d* orbitals of the alkaline-earth metal is also noted. This suggests that the Zintl formalism oversimplifies the interactions between cations and anions, and the actual bonding pictures in these compounds could be far more complicated. The states at lower energy, from -6 to -4 eV, are mainly contributed from the Al *s* orbitals and pnictogen *p* orbitals. However, comparing with states in $\text{Ba}_3\text{Al}_2\text{P}_4$ and $\text{Ba}_3\text{Al}_2\text{As}_4$ that are compressed in very narrow energy range, the states in $\text{Sr}_3\text{Al}_2\text{As}_4$ are more dispersive. Since the Al *s* and pnictogen *p* states are dominating in this range, such difference signifies different overlapping of the Al *s* and pnictogen *p* orbitals that could be attributed to the different anionic structures of the compounds, i.e., the different connectivity of the AlPn_4 tetrahedra.

The COHP diagrams are also projected in the same energy window (Fig. 5). As seen from the plots, the strongest bonding interactions are those between Al and pnictogen, in agreement with their covalent bonding character, as discussed above. The COHP curves for the *AE–Pn* interactions also show appreciable *p–d* mixing, which is indicative of some degree of covalency of the bonding between the pnictogen and alkaline-earth metal, i.e., the cations are more than just spectators and/or space fillers. Both Al–As and Sr–As interactions are optimized at the Fermi level for $\text{Sr}_3\text{Al}_2\text{As}_4$. For $\text{Ba}_3\text{Al}_2\text{P}_4$ and $\text{Ba}_3\text{Al}_2\text{As}_4$, while the Al–*Pn* interactions are optimized at the Fermi level, the Ba–*Pn* interactions remain slightly bonding character just above the Fermi level.

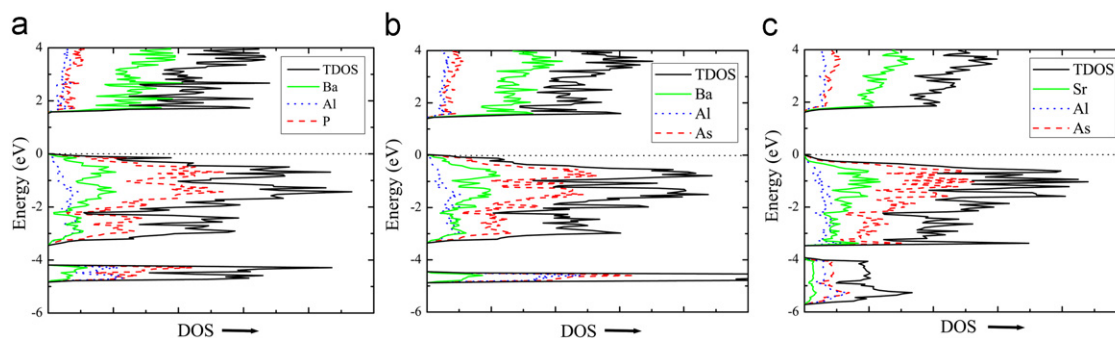


Fig. 4. DOS diagrams for (a) $\text{Ba}_3\text{Al}_2\text{P}_4$, (b) $\text{Ba}_3\text{Al}_2\text{As}_4$, and (c) $\text{Sr}_3\text{Al}_2\text{As}_4$. The Fermi level is set as the energy reference at 0 eV. On-line colors: Total DOS is shown with a black curve; partial DOS of alkaline-earth metal, Al, and the pnictogen are represented by green, blue, and red curves, respectively. (For interpretation of the references to color in this figure, the reader is referred to the web version of this article.)

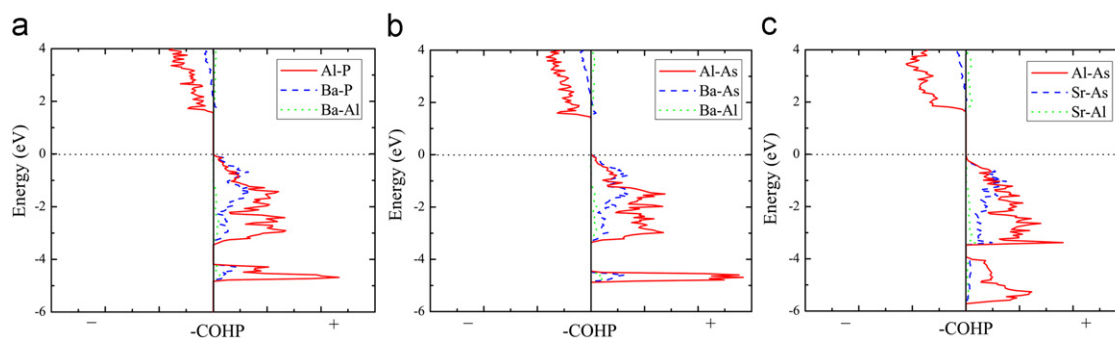


Fig. 5. COHP diagrams for (a) $\text{Ba}_3\text{Al}_2\text{P}_4$, (b) $\text{Ba}_3\text{Al}_2\text{As}_4$, and (c) $\text{Sr}_3\text{Al}_2\text{As}_4$. The Fermi level is set as the energy reference at 0 eV. On-line colors: The COHP curves of the Ba–Pn (or Sr–Pn), Al–Pn, and Ba–Al (or Sr–Al) interactions are shown in blue, red, and green, respectively. Since the “inverted” COHP values are plotted, the positive regions represent the bonding interactions, while the negative regions denote antibonding interactions. (For interpretation of the references to color in this figure, the reader is referred to the web version of this article.)

The interactions between alkaline-earth metal and Al in three compounds are all very weak.

4. Conclusions

Ten new Zintl compounds from the series of $\text{AE}_3\text{Tr}_2\text{Pn}_4$ ($\text{AE}=\text{Ca}$, Sr , Ba , Eu ; $\text{Tr}=\text{Al}$, Ga ; $\text{Pn}=\text{P}$, As) have been synthesized from flux reactions. While eight of them, $\text{Ca}_3\text{Al}_2\text{P}_4$, $\text{Sr}_3\text{Al}_2\text{As}_4$, $\text{Eu}_3\text{Al}_2\text{P}_4$, $\text{Eu}_3\text{Al}_2\text{As}_4$, $\text{Ca}_3\text{Ga}_2\text{P}_4$, $\text{Sr}_3\text{Ga}_2\text{P}_4$, $\text{Eu}_3\text{Ga}_2\text{As}_4$, and $\text{Sr}_3\text{Ga}_2\text{As}_4$ crystallize with the $\text{Ca}_3\text{Al}_2\text{As}_4$ structure type [22], the heavier alkaline-earth metal analogs, $\text{Ba}_3\text{Al}_2\text{P}_4$ and $\text{Ba}_3\text{Al}_2\text{As}_4$, adopt the $\text{Na}_3\text{Fe}_2\text{S}_4$ type structure [21]. Both structures feature corner- and edge-shared TrPn_4 tetrahedra, forming ${}^2_{\infty}[\text{TrPn}_2]^{3-}$ layers or ${}^1_{\infty}[\text{TrPn}_2]^{3-}$ chains. The title compounds are semiconductors, as it can be inferred from the valence electron count ($\text{AE}_3\text{Tr}_2\text{Pn}_4=[\text{AE}^{2+}]_3[\text{Tr}^{3+}]_2[\text{Pn}^{3-}]_4$), as well as the electronic structure calculations. Although $\text{Ba}_3\text{Ga}_2\text{P}_4$, $\text{Ba}_3\text{Ga}_2\text{As}_4$, or $\text{Yb}_3\text{Tr}_2\text{Pn}_4$ ($\text{Tr}=\text{Al}$, Ga ; $\text{Pn}=\text{P}$, As) could not be synthesized as part of this study, further exploratory work, possibly involving different synthetic approaches, will be worthwhile pursuing.

Supplementary material

The information consists of a figure showing the crystal structure of $\text{Sr}_3\text{In}_2\text{P}_4$; figures showing the experimental and simulated X-ray powder diffraction patterns of $\text{Ba}_3\text{Al}_2\text{As}_4$ and $\text{Sr}_3\text{Ga}_2\text{P}_4$; tables with the refined atomic coordinates of $\text{Ca}_3\text{Al}_2\text{P}_4$, $\text{Eu}_3\text{Al}_2\text{P}_4$, $\text{Eu}_3\text{Al}_2\text{As}_4$, $\text{Ca}_3\text{Ga}_2\text{P}_4$, $\text{Sr}_3\text{Ga}_2\text{P}_4$, $\text{Sr}_3\text{Ga}_2\text{As}_4$, and $\text{Eu}_3\text{Ga}_2\text{As}_4$; as well as tables with selected interatomic distances and angles.

Acknowledgments

Svilen Bobev acknowledges financial support from the US Department of Energy through a grant DE-SC0001360. Maia Saito acknowledges NSF REU fellowship.

Appendix A. Supplementary materials

Supplementary materials associated with this article can be found in the online version at doi:10.1016/j.jssc.2012.01.042.

References

- [1] S.J. Kim, M.G. Kanatzidis, *Inorg. Chem.* 40 (2001) 3781–3785.
- [2] I. Todorov, D.Y. Chung, L. Ye, A.J. Freeman, M.G. Kanatzidis, *Inorg. Chem.* 48 (2009) 4768–4776.
- [3] J. Mathieu, R. Achey, J.H. Park, K.M. Purcell, S.W. Tozer, S.E. Lattner, *Chem. Mater.* 20 (2008) 5675–5681.
- [4] J. Jiang, A.C. Payne, M.M. Olmstead, H.O. Lee, P. Klavins, Z. Fisk, S.M. Kauzlarich, R.P. Hermann, F. Grandjean, G.J. Long, *Inorg. Chem.* 44 (2005) 2189–2197.
- [5] J. Jiang, M.M. Olmstead, S.M. Kauzlarich, H.O. Lee, P. Klavins, Z. Fisk, *Inorg. Chem.* 44 (2005) 5322–5327.
- [6] J. Jiang, S.M. Kauzlarich, *Chem. Mater.* 18 (2006) 435–441.
- [7] A.M. Goforth, H. Hope, C.L. Condon, S.M. Kauzlarich, N. Jensen, P. Klavins, S. MaQuilon, Z. Fisk, *Chem. Mater.* 21 (2009) 4480–4489.
- [8] A. Zevalkink, E.S. Toberer, W.G. Zeier, E. Flage-Larsen, G.J. Snyder, *Energy Environ. Sci.* 4 (2011) 510–518.
- [9] E.S. Toberer, A. Zevalkink, N. Crisosto, G.J. Snyder, *Adv. Funct. Mater.* 20 (2010) 4375–4380.
- [10] E. Zintl, *Angew. Chem.* 52 (1939) 1–6.
- [11] H. Schäfer, B. Eisenmann, W. Müller, *Angew. Chem. Int. Ed. Engl.* 12 (1973) 694–712.
- [12] A.M. Goforth, P. Klavins, J.C. Fettinger, S.M. Kauzlarich, *Inorg. Chem.* 47 (2008) 11048–11056.

- [13] J. Hullmann, S.Q. Xia, S. Bobev, *Acta Crystallogr.* E63 (2007) i178.
- [14] S.Q. Xia, J. Hullmann, S. Bobev, A. Ozbay, E.R. Nowak, V. Fritsch, J. *Solid State Chem.* 180 (2007) 2088–2094.
- [15] S.Q. Xia, J. Hullmann, S. Bobev, J. *Solid State Chem.* 181 (2008) 1909–1914.
- [16] S. Bobev, J. Hullmann, T. Harmening, R. Pöttgen, *Dalton Trans.* 39 (2010) 6049–6055.
- [17] P.C. Canfield, Z. Fisk, *Philos. Magn.* B65 (1992) 1117–1123.
- [18] M.G. Kanatzidis, R. Pöttgen, W. Jeitschko, *Angew. Chem. Int. Ed.* 44 (2005) 6996–7023.
- [19] H. He, R. Stearrett, E.R. Nowak, S. Bobev, *Inorg. Chem.* 49 (2010) 7935–7940.
- [20] H. He, R. Stearrett, E.R. Nowak, S. Bobev, *Eur. J. Inorg. Chem.* (2011) 4025–4036.
- [21] K.O. Klepp, H. Boller, *Monatsh. Chem.* 112 (1981) 83–89.
- [22] G. Cordier, E. Czeck, M. Jakowski, H. Schaefer, *Rev. Chim. Miner.* 18 (1981) 9–18.
- [23] M. Somer, W. Carrillo-Cabrera, K. Peters, H.-G. von Schnering, *Z. Kristallogr.* 213 (1998) 230.
- [24] H.L. Skriver, *The L.M.T.O. Method*, Springer, Berlin, 1984.
- [25] H. He, S. Bobev, unpublished results. A description of the structure of the archetype $Ba_7Ga_4Sb_9$ can be found in Ref. [26].
- [26] G. Cordier, H. Schäfer, M. Stelter, *Z. Anorg. Allg. Chem.* 534 (1986) 137–142.
- [27] R.F. Gallup, C.Y. Fong, S.M. Kauzlarich, *Inorg. Chem.* 31 (1992) 115–118.
- [28] P. Villars, L.D. Calvert (Eds.), *Pearson's Handbook of Crystallographic Data for Intermetallic Compounds*, second ed., American Society for Metals, Materials Park, OH, USA 1991, and the desktop edition 1997.
- [29] D.R. Lide (Ed.), *CRC Handbook of Chemistry and Physics*, 83rd ed., CRC Press, 2002–2003.
- [30] [a] SMART, Bruker AXS Inc., Madison, Wisconsin, USA, 2003;
[b] SAINT, Bruker AXS Inc., Madison, Wisconsin, USA, 2003.
- [31] SADABS, Bruker AXS Inc., Madison, Wisconsin, USA, 2003.
- [32] SHEXLTL, Bruker AXS Inc., Madison, Wisconsin, USA, 2003.
- [33] L.M. Gelato, E. Parthe, *J. Appl. Crystallogr.* 20 (1987) 139–143.
- [34] O. Jepsen, A. Burkhardt, O.K. Andersen, The TB-LMTO-ASAP Program, version 4.7, Max-Planck-Institut für Festkörperforschung, Stuttgart, Germany, 1999.
- [35] O.K. Anderson, O. Jepsen, *Phys. Rev. Lett.* 53 (1984) 2571–2574.
- [36] D.D. Koelling, B.N. Harmon, *J. Phys. C: Solid State Phys.* 10 (1977) 3107–3114.
- [37] W.R.L. Lambrecht, O.K. Andersen, *Phys. Rev. B* 34 (1986) 2439–2449.
- [38] P.E. Blöchl, O. Jepsen, O.K. Andersen, *Phys. Rev. B* 49 (1994) 16223–16233.
- [39] R. Dronskowski, P.E. Blöchl, *J. Phys. Chem.* 97 (1993) 8617–8624.
- [40] J. Peters, B. Krebs, *Acta Crystallogr.* B38 (1982) 1270–1272.
- [41] B. Saparov, S. Bobev, *Inorg. Chem.* 49 (2010) 5173–5179.
- [42] G. Cordier, H. Ochmann, *Z. Naturforsch.* 43 (1988) 1538–1540.
- [43] Such topology accounts for two distinct Al–Al distances, where the shorter one measures 2.888(2) Å. Such contacts are indicating no or only very weak Al–Al interactions, since they are on par with the Al–Al distance in the *fcc* structure of the Al metal [28].
- [44] L. Pauling, *The Nature of the Chemical Bond*, Cornell University Press, Ithaca, NY, 1960.
- [45] M. Somer, W. Carrillo-Cabrera, E.M. Peters, K. Peters, H.G. von Schnering, *Z. Kristallogr.* 210 (1995) 777.
- [46] G. Cordier, G. Savelsberg, H. Schäfer, *Z. Naturforsch.* 37 (1982) 975–980.
- [47] R. Roques, R. Rimet, J.P. Declercq, G. Germain, *Acta Crystallogr.* B35 (1979) 555–557.
- [48] G. Cordier, H. Schäfer, M. Stelter, *Z. Naturforsch.* 41 (1986) 1416–1419.
- [49] G. Cordier, G.H. Schäfer, M. Stelter, *Z. Naturforsch.* 40 (1985) 1100–1104.
- [50] G. Cordier, G.H. Schäfer, M. Stelter, *Z. Naturforsch.* 42 (1987) 1268–1272.
- [51] K.H. Jost, H.J. Schulze, *Acta Crystallogr.* B25 (1969) 1110–1118.